Eminently sensitive mono-rectangular photonic crystal fiber-based sensor for cancer cell detection in THz regime

Sapana Yadav[1] · Pooja Lohia[2] · D. K. Dwivedi[1]

Abstract The present study reports a design procedure and numerical investigation of a photonic crystal fiber biosensor. The proposed sensor is consisting of irregular arranged rectangular holes. The core area has been arranged of a single rectangle for sensing the cancer cells and normal cells in the frequency range 1.0–2.5 THz. Zeonex has been utilized as a fiber material. The model has been organized and computationally investigated employing software based on the finite element method. The modeling of the designed sensor authenticates its capability in identifying cancer cells. An absorbing layer: perfectly matched layer has been used for calculating optical characteristics. It has been observed that the designed PCF sensor gives a high relative sensitivity of 81.38% for cancer cells and 65.83% for normal cells, respectively. Reduced confinement loss as 5.828×10^{-25} cm^{-1} has been achieved. Also, the effective area 2.549×10^{-8} μm^2, birefringence 4.709×10^{-4}, propagation constant 1.01961×10^{-24} and effective refractive index as 1.475×10^{-18} have been investigated. The present manufacturing technique is appropriate for the designing of proposed PCF sensor.

Keywords Relative sensitivity · Confinement loss · Birefringence · Propagation constant · Photonic crystal fiber

✉ D. K. Dwivedi
todkdwivedi@gmail.com

1 Photonics and Photovoltaic Research Lab, Department of Physics and Material Science, Madan Mohan Malaviya University of Technology, Gorakhpur 273010, India

2 Department of Electronics and Communication Engineering, Madan Mohan Malaviya University of Technology, Gorakhpur 273010, India

Introduction

Presently there is no medicine which can eradicate cancer completely. The single option to fight cancer is to diagnose it at slightly earlier stages accurately. Cancer diagnosis can be done by employing the optical and biochemical performance of cancerous cells [1]. Because various cells' responses to light are different, this property could be investigated to identify different cells proficiently. Furthermore, early cancer detection could play an important role in lowering cancer-related mortality rate. As a result, recently research related to an efficient and effective method for early cancer diagnosis has drawn much attention across the globe. In fast paced life, cancer—the unlimited development of cancer cells in the human body has taken place unhealthy, fatal illness specified by high daily death rate [2, 3]. This kind of uncontrolled tumor growth is a collaborative result of excessive interaction to toxic materials, emitting sources, and chronic materials, strong liquor consumption, greasy health, an unbalanced diet, low physical activity, nutritional insufficiency, and so on [4]. If the damaged cells are not spotted at a primitive phase, the cancer could develop all over the body, eventually killing the patient. Various blood analysis (e.g., blood protein testing, tumor marker, complete blood count, tumor marker testing etc.) and urine analysis have been generally performed to detect cancer, but the consequences could not explicitly state the negatively damaged organ [4]. Biopsy has been the standard method for recognizing cancerous cells, and it requires taking samples of suspected cells for testing [5]. Positron emission tomography (PET), ultrasound scan, magnetic resonance imaging (MRI) and computed tomography (CT) might be other prevalent tests for detecting cancer [6, 7]. Moreover, these tests have been time-consuming (varying from 2 to 30 mins to 2–3 days),

that could have negative consequences for cancer patients who require prompt diagnosis [8]. Consequently, optoelectronics researchers have been attempting to develop fast cancer cell identifiers. Cancerous and normal cells have distinct refractive indices (RIs) and show different propagation properties when light given from a similar source. Therefore, to detect the characteristics of cell could be detected by investigating the received signal [9].

The terahertz frequency spectrum has been known as the IR-microwave transmission bridge. THz waves are a subcategory of the electromagnetic spectrum from 0.1 to 10 THz frequency range. The terahertz frequency's outstanding proficiency makes it relevant in a wide area of usage. The most essential of these applications have been explosive threat detection, medical, sensing and real-time imaging, environmental [10, 11].

Photonic crystal fibers (PCF) are a kind of optical fiber in which air holes have been designed randomly or systematically across the cross section [12]. PCF not only reduces the risk of uncontrollable losses through free space [13], but these are also small, inexpensive robust, and relevantly, extremely delicate as well as relevant [14]. There have been two kinds of PCF based on their guiding techniques: photonic bandgap fibers that use the photonic bandgap mechanism [15], and index guiding fibers, which use modified total internal reflection [16]. Due to the extremely low energy of each photon, THz-based sensors have been strongly efficient of penetrating porous samples except damaging the test layer [12, 17].

The versatility in developing the cross section represents the most beneficial characteristic of PCFs which characterizes it from conventional fiber optics [18]. This enables researchers to achieve the desired waveguide characteristics, such as reduced confinement loss [19] and tremendously high sensitivity [20], high birefringence [21] and numerical aperture [22], large modal area [23], and ultra-fat near-zero dispersion [24, 25]. So, plenty of complicated PCF cross sections have been developed over the years, such as hexagon shaped [26], octagon shaped [27], spiral [28], elliptical [29], honeycomb [30], and hybrid [31] claddings.

The representative material in PCF has also been a key factor of investigations. However, metallic optical fibers were previously utilized. Current research is concentrating on optical polymers such as SILICA [32], PMMA [33], ZEONEX [34], TEFLON [35], TOPAS [36] and TELLURITE [37]. Optical polymers have been well-known for their low cost, impact resistance, and ease of integration with optical and mechanical systems [38]. THz sensors based on PCF have been broadly employed in air quality monitoring of our surroundings [39], identification of toxic substances and explosive materials such as cyanides [40], blood component evaluation [41, 42], alcohol identification in beverages [43] and leaking nature of highly flammable and dangerous

gases such as hydrogen sulfide and methane in industry sectors because of their enormous popularity.

Sharan et al. [44] proposed the photonic bandgap technique to identify cancer cells in 2014. Moreover, the photonic band gap technique has complexity in the manufacturing procedure. The thermal profile has an influence on the result. Sharma et al. [45] reported a 2D photonic crystal fiber-based sensor for the analysis of cancer cells in cervical, breast and basal cases. The working wavelength region has been extremely narrow. Furthermore, the manufacturing tolerance was not presented. Ramanujan et al. reported a geometrical covered nanocomposite material-based photonic crystal fiber for identifying cancer cells in 2018 [46]. They were using surface plasmon resonance (SPR)-based sensor and obtained extremely small sensitivity. Shimohammadli et al. [47] developed a microfluidic apparatus for analyzing breast cancer in the middle of 2018. Ayynar et al. [48] reported a dual-core PCF model that could detect breast, basal and cervical cancers during the same year. Despite the enhanced sensitivity response, the identification limit has been extremely small. Jabin et al. [49] proposed a cancer model based on surface plasmon resonance for the rapid identification of several kinds of cancer cells with enhanced sensitivity performance and identification limit in 2019. Furthermore, a novel amoeba-shaped design has been constructed, and major optical parameters have been evaluated, but the relative sensitivity performance did not come as satisfactory compared to the other parameters [50]. To overcome the ongoing difficulties and to rise the relative sensitivity the present model has been designed and analyzed. As per the knowledge of authors, eminently sensitive mono-rectangular photonic crystal fiber (MRC-PCF)-based sensor for cancer cell detection in THz region is not reported so far.

In the present work, a close-packed cladding PCF has been proposed. The proposed model is simple in structure with high relative sensitivity and reduced confinement loss which delivers simple design with enhanced outcome for the identification of cancer cells and normal cells. Several characterizations have been investigated in the proposed work like relative sensitivity, confinement loss, effective area, effective refractive index, birefringence, and propagation constant. The process for mathematically calculating the performance of the studied model is also presented in Fig.1. Finally, the results are shown, along with a conclusive analysis.

Design methodology

In this design, the finite element method (FEM) has been used. Firstly, the geometry of the model is designed. Furthermore, material has been applied as per their respective area. Zeonex is employed in the background material as well
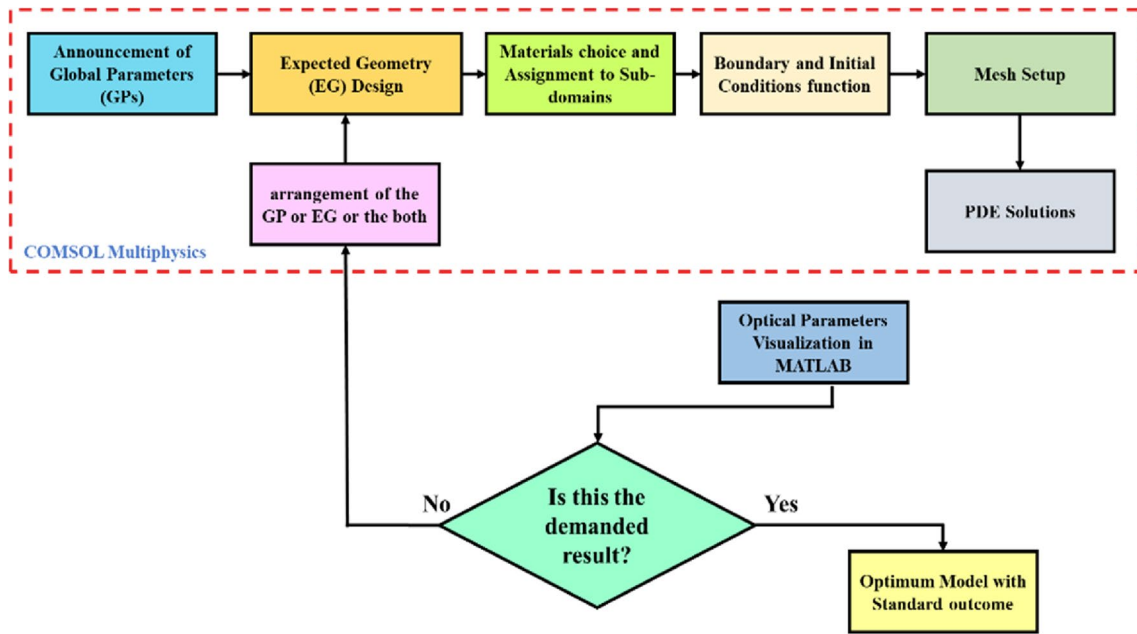
Fig.1 Schematic sketch of proposed sensor design and analysis

as perfectly matched layer (PML). Air has been inserted in the cladding region and analyte in the core region. The normal cells and cancer cells as analytes have been filled into core region. The PML aims to prevent light from reflection and to prevent the PCF from the consequences of the surrounding environment, but it makes no contribution to practical analysis. Boundary conditions have been initialized and mesh setup has been done. Thereafter, the partial differential equation (PDE) algorithm has been done. From the PDE solutions, optical performance parameters have been analyzed. This consecutive process has been shown in Fig.1.

The pictorial depiction of the constituents symbolic for our predictable MRC-PCF model has been represented in

Fig.2. The primary aim of this model is to make a unique manufacturer-friendly PCF design. A further essential aim is to obtain standard values for the optical characteristics. The PCF using only rectangles has been designed which confirms that such manufacturing is viable now. The optimized MRC-PCF shown in Fig. 2 has been observed after various investigations of altering the design (shifting the rectangle numbers, adjusting the width and length, modifying the rectangle locations, etc.). The presented MRC-PCF has a complete radius of 1750 μm and it is associated with a perfectly matched layer (PML) on the internal surface having thickness 8% of the radius. PML acts as an anti-reflection coating and avoid signals departing the fiber [51]. The core
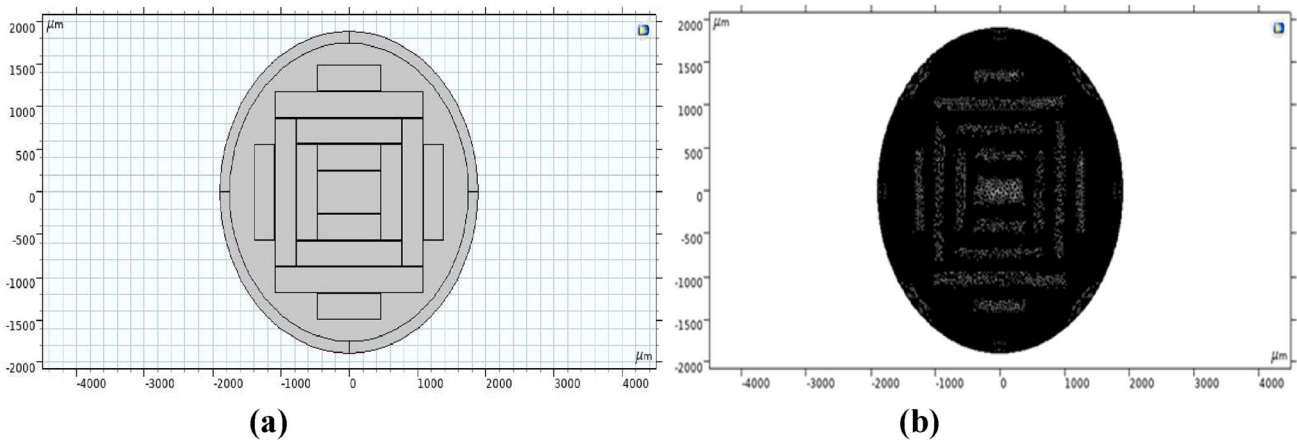
Fig.2 Configuration of the proposed PCF model **a** representative and **b** fine mesh analysis

area has been shown in the diagram by a single rectangle represented by R_c. The core's height and width have been taken as 500 and 920 μm, respectively. Fourteen rectangular air holes have been organized irregularly in the cladding region. Same symbols have been used to represent the similar rectangles. For example, the core's nearest right and left rectangles have been similar and therefore indicated by a single symbol R_1. Going to follow this strategy, designed six different rectangle structures are indicated by R_1, R_2, R_3, R_4, R_5, and R_6, the height is (H) and width is (W) for every rectangle represented in Fig.2. The studied design has a pitch of 310 μm and a strut of 10 μm between two sequential rectangles. Zeonex has been chosen as our fiber component due to its unique properties. In the THz region, Zeonex has key beneficial property as its immobile RI of 1.53. Furthermore, Zeonex has been acquired with high chemical resistance, glass transmigration warmth, and humidity insensitivity [52].

Various fabrication processes of PCF have been used so far. For example, 3D printing, extraction, Sol–gel etc. [53]. To fabricate irregular design, both extraction and 3D printing have been examined favorably. PCF designs as rectangles have already been manufactured in Planck Institute. The manufacturing viabilities of the studied optimized PCF are described in the literature [54].

Model analysis

In this study, physics-controlled mesh size is employed for better outcome. Complete mesh consists of 55584 domain elements and 3390 boundary elements of the fiber. Popular FEM has been employed for the studied PCF. Finite element method changes the microfabricated model into the ordinary differential equation. Finite element method is precise and gives designing of complicated structures before

manufacturing. It also gives the complete analysis through which the design can be enhanced. Figure 2 shows the mode field distribution at 2.1 THz frequency for normal and cancer cell as analyte and gives best result. It can be noticed from Fig.3 that field intensity is more at the midpoint and then reducing continuously within the radius of the fiber which shows a Gaussian property. It can also be noticed that light has been airtight limited within the core area, which establishes a strong interaction between material and field to be sensed. As a result, the relative sensitivity of the proposed sensor fiber would be high. For model analysis, evaluation of the waveguide characteristics against important parameter, the operating frequency of the THz range has been chosen. For analysis, x polarization has been chosen and y polarization has been ignored because light confinement has been improved significantly in the x polarization mode, with improved relative sensitivity behavior and reduced confinement loss.

Using FEM in 1.0–2.5 THz frequency range, the optimum MRC-PCF has been proposed. To analyze the performance of the model, implementing the material to be examined into the core, various performance parameters have been calculated. The relative sensitivity (RS), effective area (A_{eff}), confinement loss (CL), birefringence (B) and effective refractive index (n_{eff}), propagation constant ($β$) have been examined.

It shows that intensity of light has strong interaction with the analytes, while exhibiting less interaction in the cladding area. The results obtained for studied PCF show enhanced sensitivity. Sensitivity is directly proportional to the analytes' refractive index.

Confinement loss

The confinement loss (CL) fundamentally arises because of optical power leakage from core to cladding because of introduction of a finite air holes. The CL can be evaluated
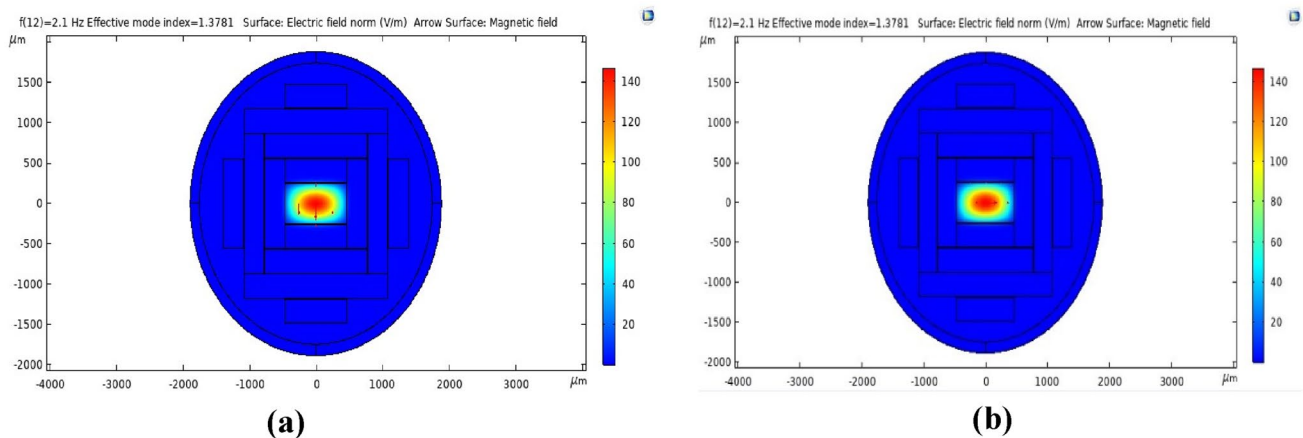

Fig.3 Mode field distribution of proposed PCF model **a** x-polarized and **b** y-polarized

using effective refractive index imaginary part. It can be lowered by appropriately ordering the core holes and cladding. The numerically CL is calculated using Eqn. (1) [55, 56].

$$CL = \frac{4\pi f}{c} \times \text{Img}(n_{\text{eff}}), \text{ cm}^{-1} \tag{1}$$

where n_{eff} and f represent the effective refractive index and frequency in THz region, respectively.

Figure 4 indicates that the confinement loss is very low. It indicates that confinement loss reduces as the frequency rises. From Fig. 4, it can be observed that an inverse relation between confinement loss and frequency holds. The confinement loss recorded at 2.1 THz frequency are 5.828×10^{-25} cm^{-1}, 3.072×10^{-27} cm^{-1} for cancer and normal cells, respectively.

Confinement loss occurs by optical mode leakage from the core of the fiber. The air holes inside the cladding region have been organized so that the refractive index difference has been sufficient to preserve the optical field within core region. Light travels away from the core and into the cladding region due to insufficient refractive index contrast, expanding confinement loss. As a result, creating effective cladding with adequate air pitch and air-hole diameter values will assist in lowering confinement loss, which may be lowered to minimal levels by appropriate cladding structure design [57–59].

Birefringence

Birefringence is the most essential parameter of optical characteristics which has been employed widely in coherent optical communications and in the manufacturing of fiber optic sensors. The electric field of a propagating electromagnetic wave has always been associated in a specific direction, which is known as polarization. When a linearly polarized light penetrates a fiber core with an anisotropic refractive index distribution, it divides into two mutually orthogonal polarized modes. These two orthogonal modes propagate at varying speeds based on the refractive index of the fiber along the direction of polarization. The birefringence is the difference in refractive indices along two mutually perpendicular directions [57]. This parameter represents the polarization-controlling ability of photonic crystal fiber. Birefringence can be evaluated using the refractive index (RI) difference between the x (n_{xplane}) and y (n_{yplane}) plane as shown in Eqn. (2) [55, 56].

$$B = \left| n_{\text{xplane}} - n_{\text{yplane}} \right| \tag{2}$$

where n_{xplane} and n_{yplane} indicate the effective refractive index of x and y polarizing modes, respectively.

From Fig.5, it is obvious that the change of birefringence can be represented with the variation of frequency range. Because of the tight confinement at higher frequencies, the refractive index mode varies in a decreasing direction after a specific frequency. The modeling of an asymmetric PCF design produces a noteworthy refractive index difference. For the studied PCF, birefringence has been obtained as 4.709×10^{-4} and 4.885×10^{-4} for cancer and normal cells, respectively.

Because the birefringence in PCFs is caused by a non-axisymmetric allocation of the effective refraction around the core, they are extremely temperature insensitive. Because of such immunity, PCF with high birefringence is very appealing for telecommunication and sensing applications. Such PCF can compensate the polarization mode dispersion in optical fibers.
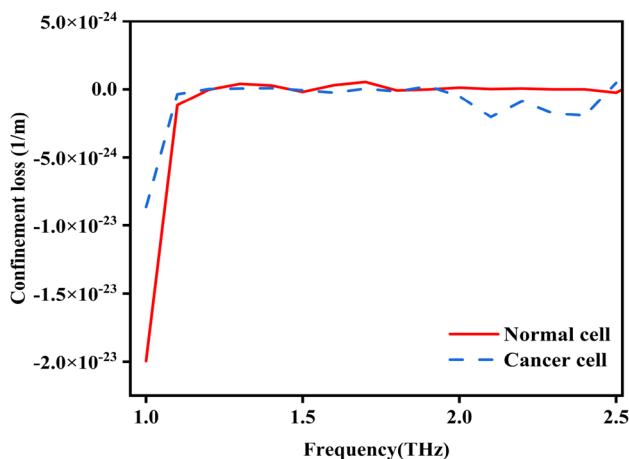
Fig.4 Confinement loss vs frequency between the cancer cell and normal cell
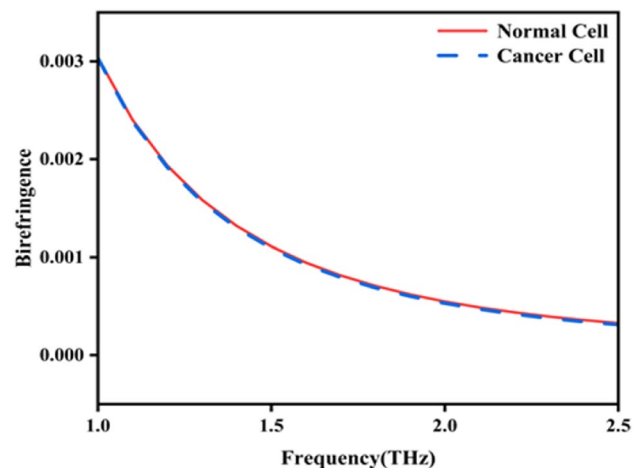
Fig.5 Birefringence vs frequency plot for the cancer cell and normal cell

Effective area

Effective area measures the analyte identification area of any PCF-based sensor. For reducing the deterioration increased by the nonlinear effect, a wide effective area is essential. A low effective area allows for the high-power density required for nonlinear impacts to be considerable. Extension of the electromagnetic wave is based on the strut size and holes size of the fiber. The mathematical parameters of the designed model can be arranged in the similar way. The effective area has been calculated as [55].

$$A_{\text{effect}} = \frac{\left(\int \int |E|^2 dxdy\right)^2}{\int \int |E|^4 dxdy} \tag{3}$$

Here, the distribution of electric field over the cross section of fiber can be represented by |E|.

From Fig.6, it is noticed that the effective area decreases as the frequency increases. With increasing frequency, it is observed that light confinement takes place through the core region, consequently lowering the effective area of the fiber. At 2.1 THz frequency, the effective area can be attained as 4.445×10^{-8} μm^2 and 2.549×10^{-8} μm^2 for normal and cancer cells, respectively.

Relative sensitivity

In MRC-PCF major light travels through the core area. A very small portion of the beam specified as the evanescent wave transfers through the cladding region and the light corresponds with the material to be sensed. The sensitivity evaluating factor measures the light interaction with the selected materials. It can be expressed using Beer–Lambert law as [55].
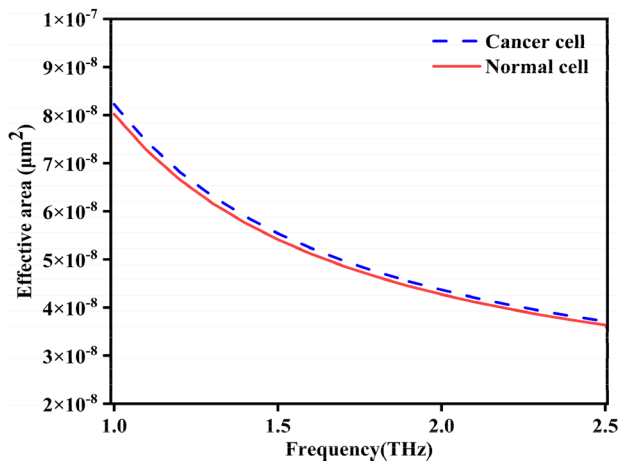
Fig.6 Effective area vs frequency for the cancer cells and normal cells

$$I(f) = I_0(f) \exp[-r\alpha_m l_c] \tag{4}$$

where $I_0(f)$ and $I(f)$ represent light intensity before and after putting the analyte at the assigned place, respectively. l_c denotes the length of the channel, α_m denotes the absorption coefficient, where l_c inversely proportional to the α_m, while f denotes the operating frequency and the relative sensitivity 'r'.

The absorbance of the liquid concentration or evanescent wave can be evaluated by Eqn. (6) [53].

$$A = \log\left[\frac{I(f)}{I0(f)}\right] = -r\alpha_m l_c \tag{5}$$

The relative sensitivity of presented PCF can be calculated by [55].

$$r = \left[\frac{n_r}{n_{\text{eff}}}\right] \times P \tag{6}$$

where n_r represents the refractive index of assigned materials, n_{eff} represents the effective refractive index of guided mode and P shows the ratio of interaction between the light intensity and directed analytes given by Eqn. (7) [55].

$$p = \frac{\int_{\text{analyte}} \text{Re}\left(E_x H_y - H_x E_y\right) dxdy}{\int_{\text{total}} \text{Re}\left(E_x H_y - H_x E_y\right) dxdy} \tag{7}$$

where E_x and E_y, H_x and H_y shows the electric field and magnetic field elements along x and y modes, respectively.

Figure 7 shows that the studied PCF gives the maximum sensitivity for cancer cell and minimum for normal cell since these holds the higher and lower refractive index, respectively. Relative sensitivity relates to the operating frequency too. With increase in frequency, compression of beam of light occurs and light is slightly constrained within the core with a high intensity which improves the light matter interaction, so sensitivity is improved. With rise in frequency the sensitivity rises till a particular frequency. Because of higher frequency, the beam of light has been more concisely constrained in the core area and strong interaction with the related analyte occurs which improves the power ratio of the core. Furthermore, with rise in frequency the refractive index also increases resulting an increase in sensitivity. The sensitivity is achieved as 81.38 and 65.83% for cancer cell and normal cells, respectively, for the designed PCF.

Effective refractive index

The effective refractive index is defined by Eq. (8) [53].
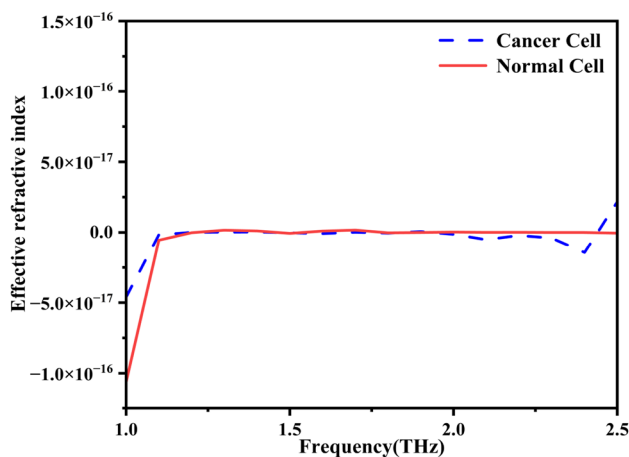
$$n_{\text{eff}} = \frac{\lambda_0}{\lambda} \tag{8}$$
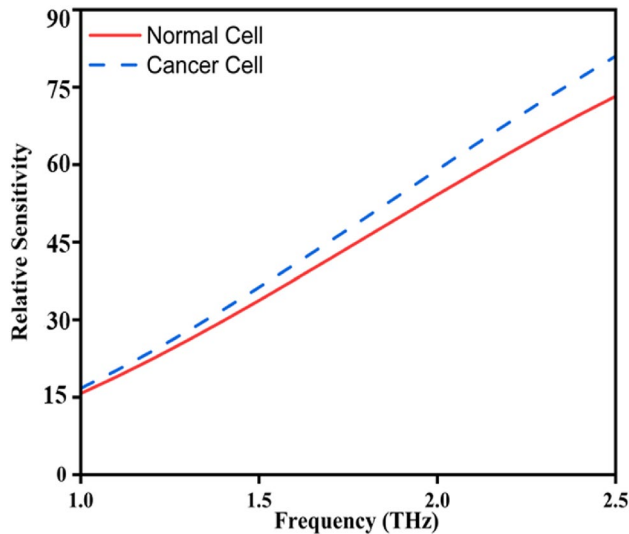
Fig.7 Relative sensitivity vs frequency between the cancer cell and normal cell

A high-refractive index core area has been bounded by a reduced refractive index material that serves as the cladding. The refractive index of the cladding has been reduced by constituting a microstructure of air holes in a predictable pattern which follows the length of the fiber. Because the interface between the reflecting core and the cladding is not made clear, the guiding principle has been the modified total internal reflection from the core and effective cladding [57].
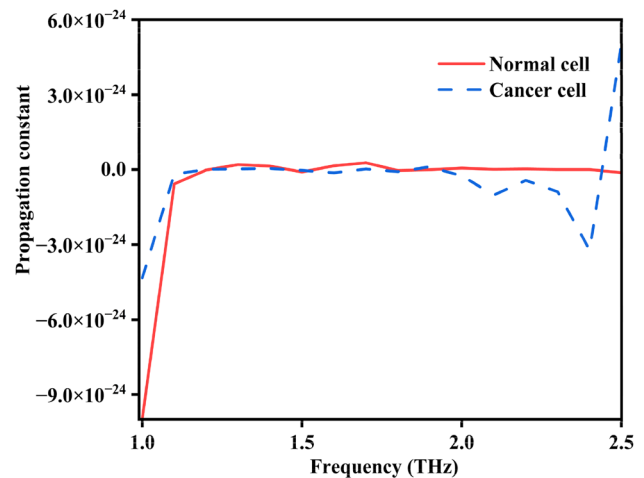
Propagation constant

To calculate the number of losses that occurs due to leakage can be predicted by propagation constant (β). Using the imaginary part of the n_{eff}, propagation constant can be evaluated with the help of Eqn. (9) [53].

$$\beta = \frac{2\pi f}{c} \text{Img}\left(n_{\text{eff}}\right) \tag{9}$$

where f denotes the frequency, Img (n_{eff}) imaginary value of n_{eff} and c speed of light.

The propagation constant is evaluated using the consistent values that arises due to the dispersion of incident light from the core to the cladding. Figure 9 shows the variation of β for the cancer cells and normal cells in the 1.0–2.5 THz frequency range. With increase in frequency, propagation constant slightly decreases then becomes almost zero. At 2.1 THz, propagation constant values are -1.01961×10^{-24} and 9.44071×10^{-27} for cancer cells and normal cells, respectively.

Here, λ represents wavelength of the em wave in the analyte and λ_0 shows the wavelength in the vacuum.

The refractive index of the core of the fiber is larger than the cladding so that the wave of the light can travel by the total internal reflection and the maximal quantity of power of the wave can be confined into the core.

Figure 8 shows the variation of the effective refractive index with frequency. Electromagnetic spectrum having larger frequency possess smaller wavelength, resulting in a larger n_{eff}, and light propagating in an analyte with a larger n_{eff} lessens the wavelength and increases the n_{eff} because of the related Eqn. (8). The n_{eff} can be achieved as 1.475×10^{-18} and 7.773×10^{-21} for cancer cell and normal cells, respectively, for the designed PCF.

Fig.8 Effective refractive index vs frequency for the cancer cells and normal cells

Fig.9 Propagation constant vs frequency for the cancer cell and normal cell
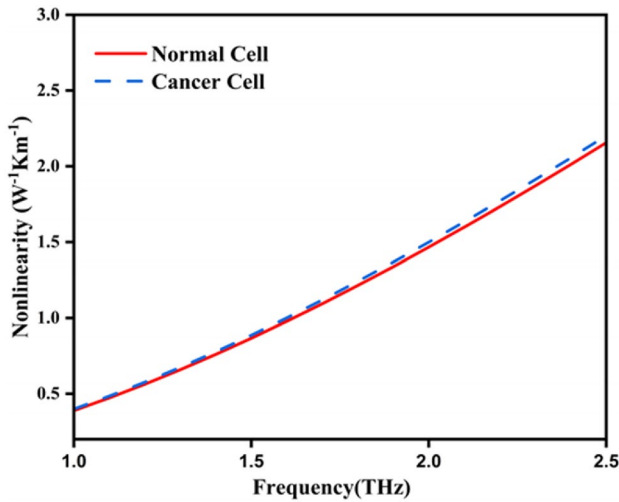
Fig.10 Nonlinearity vs frequency for the cancer cell and normal cell

Nonlinearity

The density of high optical power of fiber has been given by a low effective area for which the nonlinear effects are prominent. Nonlinearity V, known as nonlinear coefficient, calculates the capability of constraining the high-intensity light. It is defined as the inverse of the effective area of the fiber. It can be evaluated using Eq. (10) [30].

$$V = \frac{2\pi f}{c} \frac{n_2}{A_{\text{effect}}} \tag{10}$$

where n_2 shows the effective refractive index of the fiber material, A_{effect} denotes the effective area, c represents the speed of light and f represents the frequency in the THz range.

Optical nonlinearity can be employed to construct feasible optical fiber devices. By making large air holes or lowering the core dimension, PCFs could be constructed with a high-refractive index contrast between both the core and the cladding. This design promotes strong confinement of the waveguides, that increases the nonlinear coefficient [57].

Figure 10 depicts that with the increase in frequency nonlinear coefficient increases. As it follows the inverse relation to the effective area (see Fig.6). The nonlinear coefficients are 1.59833 and 1.63352 $W^{-1}Km^{-1}$ for normal and cancer cells, respectively.

Conclusion

In the present work, a square core PCF biosensor has been proposed for sensing the cancerous cells as analyte. The studied PCF model sensor shows extremely remarkable high relative sensitivity of 81.38% for cancer cells and 65.83% for normal cells. Furthermore, other noteworthy propagation characteristics—reduced confinement loss of and large effective area has been attained for the analyte at design parameters of 2.1 THz. This model has been preferably satisfactory for sensing of cancer cells and normal cells. The studied PCF gives noteworthy results and could be employed in biosensing applications.

References

1. S. Suresh, Biomechanics and biophysics of cancer cells. Acta Biomater **3**, 413–438 (2007). https://doi.org/10.1016/j.actbio.2007.04.002
2. M.J.B.M. Leon, M.A. Kabir, Design of a liquid sensing photonic crystal fiber with high sensitivity, bireferingence & low confinement loss. Sens Bio-Sensing Res **28**, 100335 (2020). https://doi.org/10.1016/j.sbsr.2020.100335
3. A. Habib, A.N.Z. Rashed, H.M. El-Hageen, A.M. Alatwi, Extremely sensitive photonic crystal fiber-based cancer cell detector in the terahertz regime. Plasmonics **16**, 1297–1306 (2021). https://doi.org/10.1007/s11468-021-01409-6
4. E.T.H. Fontham, A.M.D. Wolf, T.R. Church et al., Cervical cancer screening for individuals at average risk: 2020 guideline update from the American cancer society. CA Cancer J Clin **70**, 321–346 (2020). https://doi.org/10.3322/caac.21628
5. G.E. Dressing, P. Thomas, Identification of membrane progestin receptors in human breast cancer cell lines and biopsies and their potential involvement in breast cancer. Steroids **72**, 111–116 (2007). https://doi.org/10.1016/j.steroids.2006.10.006
6. K. Tajima, Y. Obata, H. Tamaki et al., Expression of cancer/testis (CT) antigens in lung cancer. Lung Cancer **42**, 23–33 (2003). https://doi.org/10.1016/S0169-5002(03)00244-7
7. K. Glunde, Z.M. Bhujwalla, Metabolic tumor imaging using magnetic resonance spectroscopy. Semin Oncol **38**, 26–41 (2011). https://doi.org/10.1053/j.seminoncol.2010.11.001
8. L.P. Shivangani, P.K. Singh et al., Design and modeling of reconfigurable surface plasmon resonance refractive index

sensor using Al2O3, nickel, and heterostructure BlueP/WSe2 nanofilms. J Opt (2022). https://doi.org/10.1007/s12596-022-00973-2

9. A. Umar, P. Lohia, S. Singh et al., Graphene and nickel nanomaterials based surface plasmon resonance (SPR) biosensor: a theoretical study. J Nanoelectron Optoelectron 17, 1215–1218 (2023). https://doi.org/10.1166/jno.2022.3320

10. Bulbul A.A.M., Jibon R.H., Awal M.A., et al., Toxic Chemicals Detection using Photonic Crystal Fiber in THz Regime. 2020 11th Int Conf Comput Commun Netw Technol ICCCNT 2020 2–6 (2020). https://doi.org/10.1109/ICCCNT49239.2020.9225544

11. S. Singh, P.K. Singh, A. Umar et al., 2D nanomaterial-based surface plasmon resonance sensors for biosensing applications. Micromachines 11, 1–28 (2020). https://doi.org/10.3390/mi11080779

12. J. El Haddad, B. Bousquet, L. Canioni, P. Mounaix, Review in terahertz spectral analysis. TrAC - Trends Anal Chem 44, 98–105 (2013). https://doi.org/10.1016/j.trac.2012.11.009

13. Rana S., Islam S., Sultana J., et al. A highly birefringent slotted-core THz fiber. Proc 9th Int Conf Electr Comput Eng ICECE 2016 226–229. (2017) https://doi.org/10.1109/ICECE.2016.7853897

14. K. Ahmed, F. Ahmed, S. Roy et al., refractive index-based blood components sensing in terahertz spectrum. IEEE Sens J 19, 3368–3375 (2019). https://doi.org/10.1109/JSEN.2019.2895166

15. S. Olyaee, A. Naraghi, V. Ahmadi, High sensitivity evanescent-field gas sensor based on modified photonic crystal fiber for gas condensate and air pollution monitoring. Optik (Stuttg) 125, 596–600 (2014). https://doi.org/10.1016/j.ijleo.2013.07.047

16. M.S. Islam, K.M. Samaun Reza, M.R. Islam, Topas based high birefringent and low loss single mode hybrid-core porous fiber for broadband application. Indian J Pure Appl Phys 56, 399–404 (2018)

17. T. Zhao, S. Lou, X. Wang et al., Simultaneous measurement of curvature, strain and temperature using a twin-core photonic crystal fiber-based sensor. Sensors (Switzerland) (2018). https://doi.org/10.3390/s18072145

18. A. Umar, S. Singh, S. Yadav et al., Numerical study of surface plasmon resonance biosensor using aluminium oxide and bismuth telluride nanomaterials for skin cancer cell detection. J Nanoelectron Optoelectron 17, 1655–1658 (2023). https://doi.org/10.1166/jno.2022.3358

19. M. Aliee, M.H. Mozaffari, H. Saghaei, Dispersion-flattened photonic quasicrystal optofluidic fiber for telecom C band operation. Photonics Nanostruct Fundam Appl (2020). https://doi.org/10.1016/j.photonics.2020.100797

20. M.S. Islam, C.M.B. Cordeiro, J. Sultana et al., A Hi-Bi ultrasensitive surface plasmon resonance fiber sensor. IEEE Access 7, 79085–79094 (2019). https://doi.org/10.1109/ACCESS.2019.2922663

21. M.R. Islam, M.F. Kabir, K.M.A. Talha, M.S. Arefin, Highly birefringent honeycomb cladding terahertz fiber for polarization-maintaining applications. Opt Eng 59, 1 (2020). https://doi.org/10.1117/1.oe.59.1.016113

22. T. Yasui, Y. Namihira, M.A. Hossain et al., High numerical aperture square lattice structure photonic crystal fiber for optical coherence tomography. Int Conf Adv Technol Commun (2013). https://doi.org/10.1109/ATC.2013.6698113

23. E. Coscelli, R. Dauliat, F. Poli et al., Analysis of the modal content into large-mode-area photonic crystal fibers under heat load. IEEE J Sel Top Quantum Electron 22, 323–330 (2016). https://doi.org/10.1109/JSTQE.2015.2479156

24. M. Moshiur Rahman, F. Akter Mou, M. Imamul Hassan Bhuiyan, M. Rakibul Islam, Design and characterization of a circular sectored core cladding structured photonic crystal fiber with ultra-low EML and flattened dispersion in the THz regime. Opt

25. S.M. Salimullah, M. Faisal, Ultra-wideband and coherent supercontinuum generation (near and mid-infrared) in dispersion flattened ZnGeP2 photonic crystal fiber. Alexandria Eng J 70, 289–300 (2023). https://doi.org/10.1016/j.aej.2023.03.002

Fiber Technol 55, 102158 (2020). https://doi.org/10.1016/j.yofte.2020.102158

26. M.S. Islam, J. Sultana, M. Faisal et al., A modified hexagonal photonic crystal fiber for terahertz applications. Opt Mater (Amst) 79, 336–339 (2018). https://doi.org/10.1016/j.optmat.2018.03.054

27. X. Kong, X. Li, X. Jiang, B. Tang, An ultra large negative dispersion regular octagonal PCF with liquid infiltration AOPC 2015. Adv Laser Technol Appl 9671, 96711G (2015). https://doi.org/10.1117/12.2200942

28. M. Mayilamu, J.Q. Yao, Y. Lu, Y.P. Miao, Highly nonlinear and birefringent photonic crystal fiber at 1.55 μm. Guangxue Jingmi Gongcheng/Optics Precis Eng 22, 588–596 (2014). https://doi.org/10.3788/OPE.20142203.0588

29. J. Wu, S. Li, X. Jing et al., Elliptical photonic crystal fiber polarization filter combined with surface plasmon resonance. IEEE Photonics Technol Lett 30, 1368–1371 (2018). https://doi.org/10.1109/LPT.2018.2845459

30. V. Devika, M.S.M. Rajan, Hexagonal PCF of honeycomb lattice with high birefringence and high nonlinearity. Int J Mod Phys B 34, 1–10 (2020). https://doi.org/10.1142/S0217979220500940

31. Hu D.J.J., Xu Z., Ertman S., et al. Two core photonic crystal fiber with hybrid guiding Mechanisms. 2017 Conf Lasers Electro-Optics Pacific Rim, CLEO-PR 2017 2017-Janua:1–3. (2017). https://doi.org/10.1109/CLEOPR.2017.8118922

32. S. Uddin, D.K. Singh, A solid silica core based non-linear hybrid PCF with low confinement loss. Optik (Stuttg) 127, 10399–10411 (2016). https://doi.org/10.1016/j.ijleo.2016.08.043

33. C. Markos, I. Kubat, O. Bang, Hybrid polymer photonic crystal fiber with integrated chalcogenide glass nanofilms. Sci Rep (2014). https://doi.org/10.1038/srep06057

34. M.S. Islam, J. Sultana, A. Dinovitser et al., Zeonex-based asymmetrical terahertz photonic crystal fiber for multichannel communication and polarization maintaining applications. Appl Opt 57, 666 (2018). https://doi.org/10.1364/ao.57.000666

35. M. Goto, A. Quema, H. Takahashi et al., Teflon photonic crystal fiber as Terahertz Waveguide. Japanese J Appl Physics Part 2 Lett. 43, 2–5 (2004). https://doi.org/10.1143/jjap.43.l317

36. M. Islam, J. Rahman, M. Islam, Topas based low loss and dispersion flatten decagonal porous core photonic crystal fiber for terahertz communication. Int. J. Microw. Opt. Technol 14, 62 (2019)

37. M. Klimczak, B. Siwicki, A. Heidt, R. Buczyński, Coherent supercontinuum generation in soft glass photonic crystal fibers. Photonics Res 5, 710 (2017). https://doi.org/10.1364/prj.5.000710

38. A.M.R. Pinto, M. Lopez-Amo, Photonic crystal fibers for sensing applications. J Sensors (2012). https://doi.org/10.1155/2012/598178

39. S.H. Kassani, R. Khazaeinezhad, Y. Jung et al., Suspended ring-core photonic crystal fiber gas sensor with high sensitivity and fast response. IEEE Photonics J 7, 1–9 (2015). https://doi.org/10.1109/JPHOT.2015.2396121

40. M.S. Islam, J. Sultana, A. Dinovitser et al., Sensing of toxic chemicals using polarized photonic crystal fiber in the terahertz regime. Opt Commun 426, 341–347 (2018). https://doi.org/10.1016/j.optcom.2018.05.030

41. S. Singh, A.K. Sharma, P. Lohia et al., Ferric oxide and heterostructure BlueP/MoSe2 nanostructure based SPR sensor using magnetic material nickel for sensitivity enhancements. Nanomaterials 12, 107126 (2022). https://doi.org/10.1016/j.spmi.2021.107126

42. A.M.F. Shivangani, Y. Al-Hadeethi et al., Numerical study to enhance the sensitivity of a surface plasmon resonance sensor

with BlueP/WS2-Covered Al$_2$ O$_3$-Nickel Nanofilms. Nanomaterials (2022). https://doi.org/10.3390/nano12132205

43. Islam M.S., Sultana J., Dinovitser A., et al. A novel Zeonex based photonic sensor for alcohol detection in beverages. 2nd IEEE Int Conf Telecommun Photonics, ICTP 2017 2017-Decem:114–118. (2018) https://doi.org/10.1109/ICTP.2017.8285905

44. P. Sharan, S.M. Bharadwaj, F.D. Gudagunti, P. Deshmukh, Design and modelling of photonic sensor for cancer cell detection. 2014 Int Conf IMpact E-Technology US. IMPETUS **2014**, 20–24 (2014). https://doi.org/10.1109/IMPETUS.2014.6775872

45. Sharma P., Sharan P., Deshmukh P. A photonic crystal sensor for analysis and detection of cancer cells. 2015 Int Conf Pervasive Comput Adv Commun Technol Appl Soc ICPC 2015 (2015) https://doi.org/10.1109/PERVASIVE.2015.7087208

46. N.R. Ramanujam, I.S. Amiri, S.A. Taya et al., Enhanced sensitivity of cancer cell using one dimensional nano composite material coated photonic crystal. Microsyst Technol **25**, 189–196 (2019). https://doi.org/10.1007/s00542-018-3947-6

47. V. Shirmohammadli, N. Manavizadeh, Numerical modeling of cell trajectory inside a dielectrophoresis microdevice designed for breast cancer cell screening. IEEE Sens J **18**, 8215–8222 (2018). https://doi.org/10.1109/JSEN.2018.2865699

48. M.A. Mollah, M. Yousufali, I.M. Ankan et al., Twin core photonic crystal fiber refractive index sensor for early detection of blood cancer. Sens Bio-Sensing Res **29**, 100344 (2020). https://doi.org/10.1016/j.sbsr.2020.100344

49. M.A. Jabin, K. Ahmed, M.J. Rana et al., Surface plasmon resonance based titanium coated biosensor for cancer cell detection. IEEE Photonics J (2019). https://doi.org/10.1109/JPHOT.2019.2924825

50. M.A. Jabin, Y. Luo, G.D. Peng et al., Design and fabrication of amoeba faced photonic crystal fiber for biosensing application. Sensors Actuators, A Phys **313**, 112204 (2020). https://doi.org/10.1016/j.sna.2020.112204

51. M.S. Islam, J. Sultana, J. Atai et al., Ultra low-loss hybrid core porous fiber for broadband applications. Appl Opt **56**, 1232 (2017). https://doi.org/10.1364/ao.56.001232

52. J.D. Shephard, W.N. MacPherson, R.R.J. Maier et al., Single-mode mid-IR guidance in a hollow-core photonic crystal fiber. Opt Express **13**, 7139 (2005). https://doi.org/10.1364/opex.13.007139

53. R.H. Jibon, M.E. Rahaman, M.A. Alahe, Detection of primary chemical analytes in the THz regime with photonic crystal fiber. Sens Bio-Sensing Res **33**, 100427 (2021). https://doi.org/10.1016/j.sbsr.2021.100427

54. T. Photonic, C. Fiber, An Ultra-Wideband Single-Polarization-Single-Mode. 21–22 (2020)

55. M.M.A. Eid, A.N.Z. Rashed, A.A.M. Bulbul, E. Podder, Mono-rectangular core photonic crystal fiber (MRC-PCF) for skin and blood cancer detection. Plasmonics **16**, 717–727 (2021). https://doi.org/10.1007/s11468-020-01334-0

56. S. Yadav, S. Singh, P. Lohia et al., Delineation of profoundly birefringent nonlinear photonic crystal fiber in terahertz frequency regime. J Opt Commun (2022). https://doi.org/10.1515/joc-2022-0143

57. N.K.B. Suthar, Advances in Photonic crystals and Devices (2019)

58. V.S. Chaudhary, D. Kumar, B.P. Pandey, S. Kumar, Advances in photonic crystal fiber-based sensor for detection of physical and biochemical parameters- a review. IEEE Sens J **23**, 1012–1023 (2022). https://doi.org/10.1109/JSEN.2022.3222969

59. S. Singh, A.K. Sharma, P. Lohia et al., Design and modelling of high-performance surface plasmon resonance refractive index sensor using batio3, mxene and nickel hybrid nanostructure. Plasmonics **17**, 2049–2062 (2022). https://doi.org/10.1007/s11468-022-01692-x